

## Absolute nonresonant multiphoton ionization cross section of NO at 532 nm

Chun He and Christopher H. Becker

*Molecular Physics Laboratory, SRI International, Menlo Park, California 94025*

(Received 9 September 1996)

The ion yields of NO molecules under irradiation of focused, high-intensity laser beams at 532 nm were measured by a reflecting time-of-flight mass spectrometer. The intensity distributions of the laser beams at the focal region were measured by direct imaging through a microscopic objective charge-coupled-device camera assembly. NO does not significantly fragment under high-intensity light field when examined using two laser systems with 6-ns and 35-ps pulse widths, the latter delivering a power density up to  $10^{14}$  W/cm<sup>2</sup>. The ion yield of NO at various laser power densities was measured over three orders of magnitude, ranging from the unsaturated region to the complete saturation regime. A multiphoton ionization model was used based on rate equation and perturbation theory. The four-photon nonresonant multiphoton ionization cross section for NO at 532 nm was determined to be  $(7.1 \pm 0.1) \times 10^{-117}$  cm<sup>8</sup> s<sup>7</sup> by fitting experimental data to the model. [S1050-2947(97)06102-7]

PACS number(s): 32.80.Rm

### I. INTRODUCTION

Multiphoton ionization (MPI) of atoms and molecules followed by time-of-flight (TOF) mass spectrometry has become a widely used technique because of its high sensitivity (ppm–ppb) and small sampling quantity (femtomole or less) [1–8]. Its applications range from fundamental research, such as elucidating the structure and dynamics of molecules, to industrial applications, such as quantitative trace sample analysis.

For these applications, it is desirable to know the ion yield of neutrals under the influence of a high-intensity light field, because the ion yield directly influences the sensitivity and quantitation of analytical methods. The MPI yields of atoms depend on both laser beam properties and atomic properties. From the laser beam aspect, the main influences are power density, frequency, polarization, and pulse length; from the atomic aspect, the response to the light field is generalized by an overall quantity, the  $n$ -photon cross section  $\sigma_n$ . The magnitude of  $\sigma_n$  depends on the wavelength and polarization, but does not depend on the laser power intensity [9]. The role played by each of these parameters varies with the number of photons involved in the ionization process. The cross sections are of fundamental value. By comparing the experimental values of  $\sigma_n$  with its theoretical values, we can check the correctness of the theoretical models.

Extensive experimental studies on nonresonant MPI cross sections of rare gases and metal vapor atoms make it evident that the cross section  $\sigma_n$  of an atom is determined mainly by the so-called *threshold* number of radiation quanta,  $n$ , defined by the relation

$$n = \left\{ \frac{V}{\hbar\omega} + 1 \right\}, \quad (1)$$

where  $V$  represents atomic ionization potential (IP) and  $\{x\}$  represents the integer part of  $x$  [9–12]. The integer  $n$  defines the order of the MPI process. A compilation of experimental data derived from studies on atomic MPI cross sections shows that, for a given order of MPI process, there is a

well-limited span of values for these cross sections [9]. This suggests that for nonresonant MPI IP is a primary factor in determining the rate of ionization, while the detailed spectroscopic characteristics and atomic energy structure may be secondary [3,10].

However, few studies until now have investigated ion production of *molecules* under very intense light fields. Previous research on molecules under intense light fields has concentrated on phenomena such as multiple-ionization kinetics [13–15], velocity [16–19] and angular [20] distributions of photofragmented ions, or charge distribution among molecular fragments [21–23]. The lack of information on ionization cross sections of molecules under intense light projects a clear contrast to the relatively large pool of data on atomic ionization cross sections. Attempts to derive molecular cross sections have been hindered by the photofragmentation that accompanies photoionization under intense light fields. “Counting” the photoions becomes complicated and ambiguous because of the multiple possible channels that may contribute to the final ion products [24]. To our knowledge, no multiphoton ionization cross section has so far been derived for molecules.

In previous work, we studied the effect of high light intensity (up to  $10^{14}$ – $10^{15}$  W/cm<sup>2</sup>) nanosecond and picosecond pulses on small gaseous molecules (O<sub>2</sub>, N<sub>2</sub>, CO, NO, and CO<sub>2</sub>) [25]. Generally, the experimental results showed that photofragmentation of these molecules under such high light fields is significant. Molecular photofragmentation is mixed with photoionization and the process is molecular specific [26]. The detailed electronic state structure of both the neutrals and ions are crucial in determining the photoionization and photofragmentation patterns of these molecules. We also concluded that at the pulse range we studied (ns to ps) both photon energy and the pulse length are important in governing the photoionization and photofragmentation pathways. However, we observed that NO is extraordinarily stable under the irradiation of high-intensity light when examined with 6-ns and 35-ps lasers at 532 nm. Unlike other molecules studied, NO photofragmentation was negligible even at the highest laser power applied. Motivated by the “atomiclike”

character of NO, we conducted the nonresonant MPI measurements described in this paper using powerful ns and ps pulses at 532 nm.

## II. EXPERIMENT

The experimental apparatus have been described elsewhere [3], so only features relevant to the present experiments are described. We performed our experiments in an ultrahigh vacuum (UHV) chamber equipped with a high-power, 10-Hz, 35-ps Nd:YAG laser having a highest 532-nm output pulse energy of 44 mJ, and a moderate power, 10-Hz, 6-ns Nd:YAG laser having a highest 532-nm output pulse energy of 520 mJ. The stainless steel chamber is pumped by a 500 l/s cryogenic pump and has a base pressure of  $1 \times 10^{-9}$  torr without bakeout. Mass spectra were recorded using a reflecting TOF system of 2-m effective path length with a mass resolution better than 1000.

Laser beam focusing was by a 10-cm focal length, best-form lens situated at the end of a tube inserted into the UHV chamber; the lens also served as an air-vacuum window. For optimal positioning of the laser focus with respect to the fixed mass spectrometer, the lens tube insert was mounted on a precision  $xyz$  vacuum manipulator via a flexible metal bellows. The laser beam travels parallel to the repeller surface of the TOF mass spectrometer and normal to the axis of the mass spectrometer. Alignment of the focus with the ion optics of the mass spectrometer is performed by leaking  $1 \times 10^{-7}$  torr Ar gas into the chamber and maximizing the  $\text{Ar}^{2+}$  (6-ns laser) and  $\text{Ar}^{3+}$  (35-ps laser) signals in the mass spectra. Photoion detection is analog by ion impact on chevron microchannel plates at 2.4-keV impact energy, followed by a 100-MHz transient digitizer coupled to a laboratory computer.

Laser beam diagnostics were performed by picking off and directing a small amount of the 532-nm beam prior to focus, and directing the laser beam through an identical best-form lens and then into a microscope objective charge-coupled-device (CCD) camera assembly mounted on a precision motion  $xyz$  stage. The intensity of the laser beam used for imaging diagnostics was adjusted by neutral density filters. The microscope objective enlarges the beam cross section at its focus plane by a fixed magnification before it is directed into the CCD camera. The magnification of the microscope objective and CCD camera assembly was determined and verified by imaging a standard test target and pinholes with known diameters. The resulting images are examined by a TV monitor through a video processing module interfaced to a laboratory computer by a frame grabber.

NO was leaked into the chamber through a gas doser controlled by a leak valve. Pressure is read from an ionization gauge and corrected to a sensitivity factor of 1.2 as the gauge is calibrated to  $\text{N}_2$ .

## III. RESULTS AND DISCUSSION

In this section we first examine the laser beam profiles at focus and the near focal region as displayed by the images acquired by the CCD camera. We determine and characterize the focused beam profile, which is a Gaussian, with beam radius  $\omega_0$  and power density  $P$ . In the second part of this

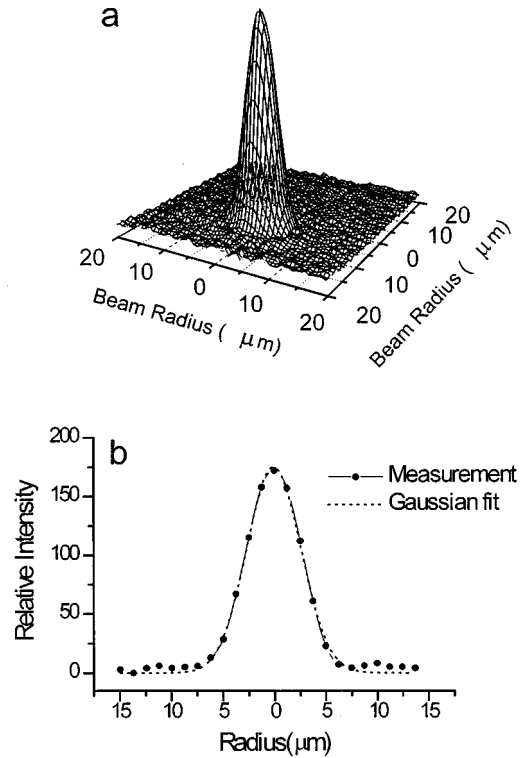


FIG. 1. (a) Laser intensity profile at the focus of a single pulse, when the beam is focused by a 10-cm best-form thin lens. (b) Projection of intensity profile on a two-dimensional plane. The dotted line represents a best Gaussian fit.

section we report the experimental data of NO, with calibrated laser power densities. Then we present an analytical expression of MPI yield based on rate equation and perturbation theory, and calculate ion yield curves of various MPI orders. Finally we apply the theory to the experimental data and derive the cross section of NO using nonlinear least-squares fit. The results suggest that the MPI theory is adequate in describing the high-intensity photoionization of NO.

### A. Laser intensity distribution

Figure 1(a) shows an intensity map of the laser beam image at the focal plane acquired by the CCD camera, and Fig. 1(b) shows a planar cut through this distribution. The dotted line in Fig. 1(b) represents a Gaussian fit. The beam waist  $\omega_0$ , measured at  $1/e^2$  of the peak intensity, is  $5.3 \mu\text{m}$ , which is very close to the value of  $5 \mu\text{m}$  calculated using Gaussian beam focusing theory with a pre-lens beam diameter of 6 mm and a 10-cm focal-length thin lens [27]. This result demonstrates that the laser has near-Gaussian and near-diffraction-limited beam profile at focus. Beam intensity images at the near focus region, which are used to obtain a three-dimensional intensity distribution, are acquired by translating the  $xyz$  stage along the axis of the laser beam. The results show that the variation of beam waist at the near focus region is well represented by a hyperbolic curve, as expected. The high-quality beam characteristics were specifically beneficial to our study not only because the saturation intensity and ion yield can be expressed quantitatively as a

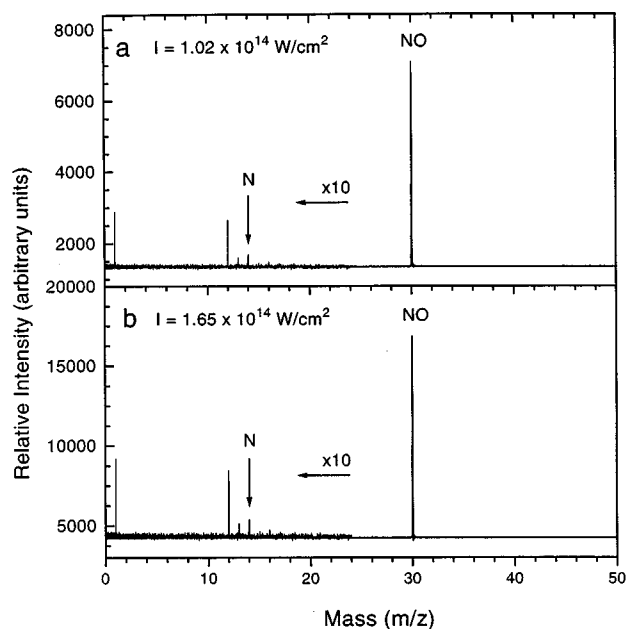


FIG. 2. High-intensity nonresonant multiphoton ionization TOF mass spectra of NO, measured at laser power densities of (a)  $1.02 \times 10^{14} \text{ W/cm}^2$  and (b)  $1.65 \times 10^{14} \text{ W/cm}^2$ . The pressure of NO is  $5.3 \times 10^{-7}$  torr. The spectra are 200-shot averages with 30-dB signal attenuation. The baseline of the analog signal is arbitrary, but is the same for all spectra.

function of laser power density, but also because almost all the theories of high-intensity laser photoionization are based on the assumption that the photon flux used has a Gaussian profile.

The pulse energies  $E$  of the lasers can be explicitly converted into power densities  $P$  or photon flux  $\Phi$  densities by using the beam parameters and the pulse durations:

$$\begin{aligned} P \text{ (W/cm}^2\text{)} &= 1.93 \times 10^{11} E \text{ (mJ/pulse)} \quad (6 \text{ ns}), \\ P \text{ (W/cm}^2\text{)} &= 3.30 \times 10^{13} E \text{ (mJ/pulse)} \quad (35 \text{ ps}), \end{aligned} \quad (2)$$

and

$$\begin{aligned} \Phi \text{ (photons/cm}^2\text{ s)} &= 5.16 \times 10^{29} E \text{ (mJ/pulse)} \quad (6 \text{ ns}), \\ \Phi \text{ (photons/cm}^2\text{ s)} &= 8.84 \times 10^{31} E \text{ (mJ/pulse)} \quad (35 \text{ ps}). \end{aligned} \quad (3)$$

The averaged power density or averaged flux density over the beam waist at focus is used to characterize the laser focus.

### B. Results of multiphoton ionization of NO

Figure 2 presents two mass spectra of NO taken at two laser power densities,  $1.1 \times 10^{14} \text{ W/cm}^2$  and  $1.7 \times 10^{14} \text{ W/cm}^2$ . The laser pulse duration was 35 ps. NO does not fragment significantly under these conditions as evidenced by the low amounts of  $\text{N}^+$  and  $\text{O}^+$ . In fact, the power density was determined by laser intensity variation to be in the saturation regime, where almost all molecules within the focal volume are ionized. (As the laser intensity increases, the size expansion of the focal volume causes the ionization yield to increase [28].)

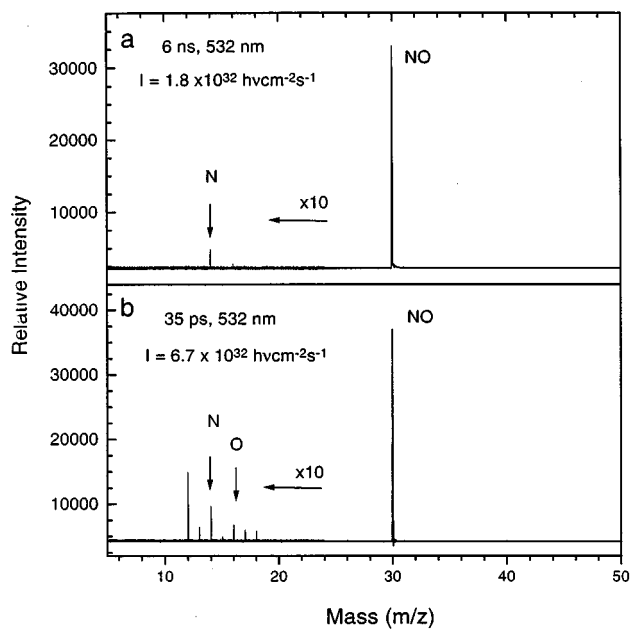


FIG. 3. TOF mass spectra of NO obtained from (a) a 6-ns, 532-nm laser and (b) a 35-ps, 532-nm laser.

Similar mass spectra were obtained using the 6-ns laser radiation (Fig. 3). The top spectrum was obtained using the 6-ns laser with a flux density of  $1.8 \times 10^{32} \text{ h}\nu \text{ cm}^{-2} \text{ s}^{-1}$ , and the bottom spectrum was obtained using the 35-ps laser with a flux density of  $6.7 \times 10^{32} \text{ h}\nu \text{ cm}^{-2} \text{ s}^{-1}$ . Note that the two spectra have similar ion yields although acquired with different laser flux (or power) densities. The two spectra were taken with a similar  $\pi(\Phi)^n$  value of  $\sim 7 \times 10^{120} \text{ h}\nu \text{ cm}^{-8} \text{ s}^{-3}$ , where  $\tau$  is the laser pulse duration,  $\Phi$  is the laser flux density, and  $n$  is the order of the MPI and has a value of 4 for NO with 532-nm photons irradiation.

The ion yield as a function of laser power density is plotted in Fig. 4. The open circles are experimental data. The laser power densities are varied from  $3 \times 10^{12} \text{ W/cm}^2$  to  $1 \times 10^{14} \text{ W/cm}^2$ , and the corresponding NO ion yield varies from 90 counts to  $1.4 \times 10^5$  counts (arbitrary unit). At lower power densities the data fall into a straight line as anticipated showing the unsaturated region. A linear least-squares fit

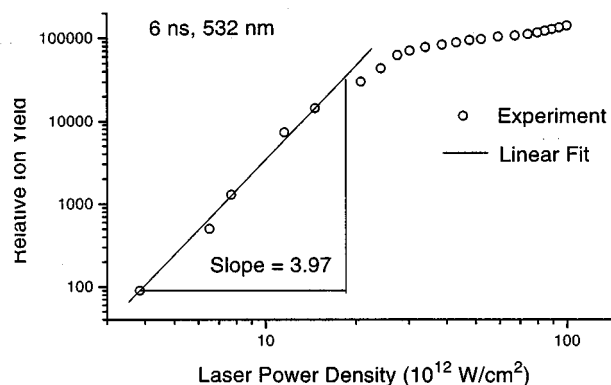


FIG. 4. Log-log plot of the variation of the ion signal intensity as a function of the laser power density  $P$  for NO.

gives a slope of 3.97, which confirms the photoionization of NO is a fourth-order process.

### C. Theoretical model

Theoretical description of the interaction of atoms with intense laser fields fall into two regimes, MPI and tunneling ionization. In the former, ionization is described by perturbation theory, and in the latter ionization is described as an ac tunneling process over atomic potential barriers. The two regimes are differentiated by the Keldysh  $\gamma$  parameters [26].

$$\gamma = \left( \frac{V}{2U} \right)^{1/2}, \quad (4)$$

where  $V$  is the zero-field ionization potential and  $U$  is the ponderomotive potential of the laser. The ponderomotive potential is the average kinetic energy of an electron and is given explicitly by

$$U \text{ (eV)} = 9.33 \times 10^{-14} I \text{ (W/cm}^2\text{)} \lambda \text{ (\mu m)} \quad (5)$$

The MPI regime corresponds  $\gamma$  value  $>1$  and the tunneling ionization regime  $\gamma < 1$ . The  $\gamma$  values corresponding to the laser power densities used in the data reduction are between 7.65 ( $I = 3 \times 10^{12}$  W/cm<sup>2</sup>) and 1.32 ( $I = 1 \times 10^{14}$  W/cm<sup>2</sup>), indicating that the MPI model is more appropriate for describing the experimental results.

The model developed for the experiment is a kinetic model based on single ionization with an ionization rate given by perturbation theory. From perturbation theory, the relationship between the ionization rate and the laser flux intensity below saturation is [9,28,29]

$$\Gamma = \sigma_n \Phi^n, \quad (6)$$

where  $\Gamma$  the ionization rate in units of  $s^{-1}$  and  $\Phi(x, y, z, t)$  is the photon flux density in units of  $h\nu \text{ cm}^{-2} \text{ s}^{-1}$ , and  $\sigma_n$  is the cross section in units of  $\text{cm}^{2n} \text{ s}^{2n-1}$ .

The ionization rate determines the ion production rate, or ion yield, with which the ion concentration  $N_i$  grows at a given point in space:

$$\frac{dN_i}{dt} = \Gamma(N_0 - N_i), \quad (7)$$

where  $N_0$  is the initial concentration of neutral atoms. Within the laser pulse duration  $T$ , the ion yield reaches the value

$$N_i = N_0 \left[ 1 - \exp\left(-\int_T \Gamma dt\right) \right], \quad (8)$$

while the total number of ions produced within the whole volume of laser profile  $S$  is

$$N_i = N_0 \int_S \left[ 1 - \exp\left(-\int_T \Gamma dt\right) \right] dx dy dz. \quad (9)$$

When the laser is operated in the TEM<sub>00</sub> mode, the spatial and temporal distributions of the laser flux density can be separated and expressed as

$$\Phi(x, y, z, t) = I_m F(x, y, z) G(t), \quad (10)$$

where  $I_m$  is the maximum intensity,  $F$  is the function giving, in relative values, the intensity at the point  $(x, y, z)$  normalized to unity at  $(0, 0, 0)$ , and  $G$  is the normalized temporal intensity distribution. Therefore, the time integration over ionization rate can be simplified as [28]

$$\int_T \Gamma dt = \sigma_n I_m^n F^n(x, y, z) \tau_n, \quad (11)$$

where

$$\tau_n = \int_T G^n(t) dt = 2^{n-1} \frac{(n-1)!}{(2n-1)!} \tau \quad (12)$$

and

$$\tau = \int_T G(t) dt. \quad (13)$$

If we define saturation intensity  $I_{sat}$  as the intensity at the spatial peak of the pulse ( $F = 1$ ) for which the argument of the exponential reaches unity,

$$\sigma_n I_{sat}^n \left( 2^{n-1} \frac{(n-1)!}{(2n-1)!} \right) \tau = 1, \quad (14)$$

the ion yield can be expressed as

$$N_i = N_0 \int_S \left\{ 1 - \exp\left[-\left(\frac{I_m F(x, y, z)}{I_{sat}}\right)^n\right] \right\} dx dy dz. \quad (15)$$

When the focusing lens is spherical, the normalized intensity distribution function  $F(x, y, z)$  is symmetric about the beam propagation direction  $z$  and Eq. (15) can be rewritten as

$$N_i = N_0 2\pi \int_S \left\{ 1 - \exp\left[-\left(\frac{I_m F(r, z)}{I_{sat}}\right)^n\right] \right\} r dr dz. \quad (16)$$

Practically, not all the ions produced are detected because of the limited aperture size of the ion optics of the TOF mass spectrometer, the less than 100% transmittance of the spectrometer, and the analog detection of the ion signal. If we generalize these effects by an overall detector gain factor  $A$ , the ion signal intensity  $I_i$  is

$$I_i = AN_i = AN_0 2\pi \int_S \left\{ 1 - \exp\left[-\left(\frac{I_m F(r, z)}{I_{sat}}\right)^n\right] \right\} r dr dz. \quad (17)$$

When the spatial distribution  $F(r, z)$  is known, Eq. (17) provides a direct comparison of the experimental results with the theory. The integration is over the space within which the ions are detected.

Figure 5 shows MPI yields as a function of the laser density for various  $n$ th-order processes, at 532-nm radiation with 6-ns pulse width. The calculation is based on Eq. (17) with beam parameters obtained from the beam diagnostic measurement and a beam truncation of 4 mm along the  $z$  (laser propagating) direction. The cross sections  $\sigma_n$  used are from Ref. [9].

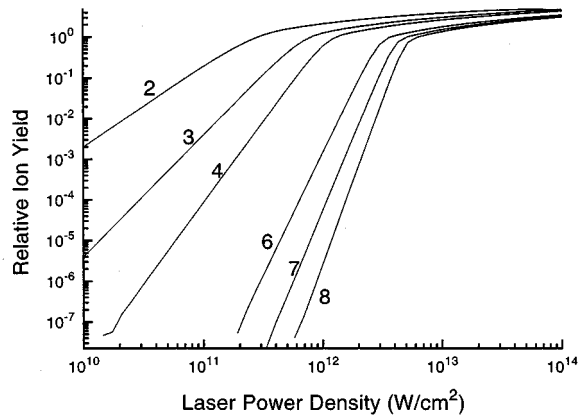


FIG. 5. Relative ion yields as a function of laser power density for different orders of nonresonant multiphoton ionization processes, calculated using Eq. (17).

#### D. Cross section of NO

Because the experimental data extend into both the unsaturated and saturated regions, fitting the data to the model expressed in Eq. (17) and plotted in Fig. 5 eliminates the need for absolute knowledge of the number of ions formed. The overall gain factor  $A$  and the cross section  $\sigma_n$  can be adjusted independently to achieve the fit. The nonlinear fitting procedure used here is Margquardt method [30].

Special attention was paid on the ionization volume, which defines the integral in Eq. (17). Because of the confined geometry of the electrostatic optics of the TOF mass spectrometer, not all the ions generated were collected. We performed ion trajectory calculations based on electrostatic fields produced by our ion extraction optics, using the SIMION 4.0 program [31] to access the segment of the ionization volume within which the ions are extracted into the TOF mass spectrometer and detected. The results show a sharp truncation along the laser beam propagation direction defined by the size of the aperture of the ion extractor. This truncation in turn can be defined by the spatial distribution function  $F(r, z)$  as

$$F(r, z) = \begin{cases} F(r, z) & |z| \leq z_{\text{crit}} \\ 0 & |z| \geq z_{\text{crit}} \end{cases}, \quad (18)$$

where  $z_{\text{crit}}$  is a critical value of  $z$  determined by the aperture of the ion extractor of the TOF mass spectrometer.

The experimental data and the result of data fitting are presented in Table I and plotted in Fig. 6. The agreement between the experimental data and the calculated curve is excellent, judging both from a visual inspection of Table I and Fig. 6 and from the  $\chi^2$  value of 0.159 from the fitting procedure [30]. The cross section of  $(7.1 \pm 0.1) \times 10^{-117} \text{ cm}^8 \text{ s}^7$  is also in the range of the cross sections measured for four-photon ionization of atoms listed in Table 2 of Ref. [9].

#### E. Discussion

The electronic spectrum of nitric oxide has been extensively studied [32] and its excited states are among the best known of any molecule. Its ground-state electronic structure consists of a single loosely bound electron outside of a filled

TABLE I. Experimental and nonlinear least-squares fitted values of NO MPI yields at different laser power densities.

Laser power density ( $10^{12} \text{ W/cm}^2$ )	Experiment	Theoretical fit
100.1	139 920	124 517
94.3	132 720	121 781
89.1	126 590	119 170
84.5	121 030	116 718
79.9	115 700	114 128
74.3	110 500	110 792
67.4	106 370	106 283
59.3	103 050	100 395
52.2	95 920	94 500
47.7	93 330	90 415
43.1	87 520	85 728
38.7	82 390	80 751
34.1	77 210	74 934
30.2	70 040	69 281
27.5	61 970	64 177
24.3	43 340	55 089
20.8	29 930	41 014
14.6	14 290	14 275
11.5	7 200	5 994
7.7	1 280	1 233
6.5	500	637
3.8	90	78

core. We speculate the observed stability of NO is originated from  $\text{NO}^+$ , which has a closed-shell electronic configuration. Studies on the ionization and dissociation dynamics of  $\text{N}_2$ ,  $\text{O}_2$ , and CO molecules concluded that the atomic ions are fragmented from their parents singly and multiply charged ions [16–18].

Because nitric oxide is essentially the molecular analogue of an alkali atom, the excited states consist largely of Rydberg states, where the weakly bound electron is in an atomiclike orbital. Almost uniquely among molecules, the electron transition probabilities follow atomiclike selection rules, tempered by molecular angular momentum constraints,

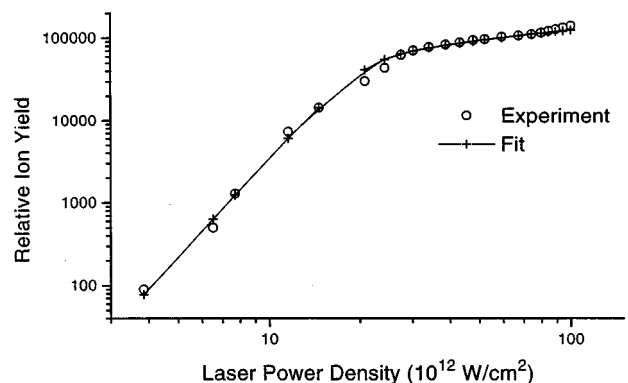


FIG. 6. Experimental data of NO ion yields and theoretical fitted values using Eq. (17) as a function of laser power density  $P$ .

with the highest occupied orbital in the ground state acting very much like a  $d$  orbital.

With an equivalent energy of 2.33 eV for the 532-nm photons, two-photon resonance channel in the four-photon ionization of nitric oxide is immediately eliminated because the lowest excited state of NO, the  $A^2\Sigma^+$  state, has a state origin  $T_e=43\,965.7\text{ cm}^{-1}$ , or 5.451 eV [33]. However, there are potentially intermediate photon-electron state interactions at three-photon resonance with low vibrational bands of  $C^2\Pi^+$  and  $D^2\Sigma^+$  states in the  $np$  Rydberg series and very high vibrational bands of  $B^2\Pi^+$  state [33]. These interactions impose the possible existence of channels of both resonance enhancement of the four-photon ionization and photodissociation. Detailed examination by Guest and Lee [34] on the absorption and fluorescence studies of NO between 6.358 and 9.183 eV show that the summed energy of three photons slightly overlaps with  $B^2\Pi^+(12)\leftarrow X^2\Pi^+(0)$  band. The  $B^2\Pi^+$  state of NO is known to predissociate strongly above the first dissociation limit (6.478 eV) [33]. The observed atomiclike characteristics of NO under high laser intensity MPI is probably due to the long lifetime of  $\geq 14$  ns of the  $B^2\Pi^+(12)$  state compared with the MPI process [35].

Zakheim and Johnson [36] studied two-photon and three-photon resonances in the four-photon ionization spectrum of nitric oxide, using a nitrogen laser pumped dye laser. The characteristics of the dye laser was 6 ns in pulse width, 1–2  $\text{cm}^{-1}$  in bandwidth, and a maximum power density of about  $10^{10}\text{ W/cm}^2$ . The laser was scanned between 405 and 485 nm to meet resonances at three-photon energies. The resulting three-photon resonance, four-photon ionization cross sections vary from  $2\times 10^{-102}$  to  $5\times 10^{-100}\text{ cm}^8\text{ s}^7$ , depending on energy levels in resonance [36,37]. These values are much larger than the cross section we obtained here.

It is worth mentioning that the 6-ns pulses of the  $Q$ -switched Nd:YAG laser used in the present experiment contain multiple modes fluctuating in intensity randomly with time, which is obviously in conflict with the assumption of a steady, hyperbolic-secant-squared temporal profile used

to derive Eqs. (12) and (13). In this regard, the correspondence between results shown in Fig. 3, obtained with the two lasers, is to some degree fortuitous. The ideal approach is to perform a measurement of the laser temporal distributions for a statistically large enough number of pulses. The averaged value of subsequent temporal integrations of the pulses should be used to replace the  $\tau_n$  value used in Eqs. (11) and (12).

#### IV. CONCLUSIONS

We examined the nonresonant multiphoton ionization of NO using TOF mass spectrometry at  $\lambda=532\text{ nm}$  as a function of laser power density in the range of  $10^{12}\leq P\leq 10^{15}\text{ W/cm}^2$  using a 6-ns and a 35-ps Nd:YAG laser. To quantitatively facilitate this investigation, we acquired intensity distribution profiles of the laser beam at its focus and near focal regions. The three-dimensional intensity images show near-Gaussian, near-diffraction-limited light intensity distributions. NO does not fragment when the power density reaches  $10^{14}\text{ W/cm}^2$ . The extraordinary stability of NO enables us to extract the MPI cross section of NO and makes it possible to directly compare the experimentally measured ion yields with those predicted by theory. We developed a rate equation kinetic model of multiphoton ionization, which assumes single ionization by a direct process to determine the MPI cross section. We found that the cross section of nonresonant multiphoton ionization of NO is very close to the values obtained for atoms that require four-photon ionization.

#### ACKNOWLEDGMENTS

The authors acknowledge financial support from the Chemistry Division of the National Science Foundation, Grant No. CHE-9321742. We thank Dr. Tom Slanger for useful discussion about the spectroscopy of NO and Lei Fu for his generous help in programming the code for data fitting.

- 
- [1] P. Williams, *Appl. At. Collision Phys.* **4**, 327 (1983).  
 [2] C. R. Brundle, C. A. Evans, Jr., and S. Wilson, *Encyclopedia of Materials Characterization* (Butterworth-Heinemann, Boston, 1992).  
 [3] Chun He and C. H. Becker, *Surf. Interface Anal.* **26**, 79 (1996).  
 [4] M. L. Wise, A. B. Emerson, and S. W. Downey, *Anal. Chem.* **67**, 4033 (1995).  
 [5] N. Winograd, *Anal. Chem.* **65**, 622A (1993).  
 [6] C. R. Ayre, L. Moro, and C. H. Becker, *Anal. Chem.* **66**, 1610 (1994).  
 [7] R. Moller, M. Terhorse, E. Niehuis, and A. Benninghoven, *Org. Mass Spectrom.* **27**, 1393 (1992).  
 [8] C. Trappe, M. Schutze, M. Raff, R. Hannot, and H. Kurz, *Fresenius J. Anal. Chem.* **346**, 368 (1994).  
 [9] M. V. Ammosov, N. B. Delone, M. Yu. Ivanov, I. I. Bondar, and A. V. Masalov, in *Advances in Atomic, Molecular, and Optical Physics*, edited by D. Bates and B. Bederson (Academic Press, Boston, 1992), Vol. 29, p. 33.  
 [10] G. Mainfray and C. Manus, *Rep. Prog. Phys.* **54**, 1333 (1991), and references therein.  
 [11] M. D. Perry, A. Szöke, O. L. Landen, and E. M. Campbell, *Phys. Rev. Lett.* **60**, 1270 (1988).  
 [12] D. Charalambidis, P. Lampropoulos, H. Schröder, O. Faucher, H. Xu, M. Wagner, and C. Fotakis, *Phys. Rev. A* **50**, R2822 (1994).  
 [13] K. Boyer, T. S. Luk, J. C. Solem, and C. K. Rhodes, *Phys. Rev. A* **39**, 1186 (1989).  
 [14] P. A. Hatherly, M. Stankiewicz, K. Codling, L. J. Frasinski, and G. M. Cross, *J. Phys. B* **27**, 2993 (1994).  
 [15] J. Purnell, E. M. Snyder, S. Wei, and A. W. Castleman, Jr., *Chem. Phys. Lett.* **229**, 333 (1994).  
 [16] C. Cornaggia, J. Lavancier, D. Normand, J. Morellec, and H. X. Liu, *Phys. Rev. A* **42**, 5464 (1990).  
 [17] J. Lavancier, D. Normand, C. Cornaggia, J. Morellec, and H. X. Liu, *Phys. Rev. A* **43**, 1461 (1991).

- [18] D. Normand, C. Cornaggia, J. Lavancier, J. Morellec, and H. X. Liu, *Phys. Rev. A* **44**, 475 (1991).
- [19] L. J. Frasinski, K. Codling, P. Hatherly, J. Barr, I. N. Ross, and W. T. Toner, *Phys. Rev. Lett.* **58**, 2424 (1987).
- [20] P. A. Hatherly, L. J. Frasinski, K. Codling, A. J. Langley, and W. Shaikh, *J. Phys. B* **23**, L291 (1990).
- [21] M. Stankiewicz, L. J. Frasinski, G. M. Cross, P. A. Hatherly, K. Codling, A. J. Langley, and W. Shaikh, *J. Phys. B* **26**, 2619 (1993).
- [22] C. Cornaggia, M. Schmidt, and D. Normand, *J. Phys. B* **27**, L123 (1994).
- [23] L. J. Frasinski, P. A. Hatherly, K. Codling, M. Larsson, A. Person, and C.-G. Wahlström, *J. Phys. B* **27**, L109 (1994).
- [24] K. Codling and L. J. Frasinski, *J. Phys. B* **26**, 783 (1993).
- [25] C. He, J. Basler, A. Paul, and C. H. Becker, *J. Vac. Sci. Technol. A* **14**, 1433 (1996).
- [26] L. V. Keldysh, *Sov. Phys. JETP* **20**, 1307 (1965).
- [27] A. E. Siegman, *Lasers* (University Science Books, Mill Valley, CA, 1986), Chap. 17.
- [28] M. D. Perry, O. L. Landen, A. Szoke, and E. M. Campbell, *Phys. Rev. A* **37**, 747 (1988).
- [29] A. l'Huillier, L. A. Lompre, G. Mainfray, and C. Manus, *Phys. Rev. A* **27**, 2503 (1983).
- [30] W. H. Press, S. A. Teukosky, W. T. Vetterling, and B. P. Flannery, *Numerical Results in Fortran*, 2nd ed. (Cambridge University Press, Cambridge, 1992).
- [31] D. A. Dahl and J. E. Delmore, SIMION 4.0, PC/PS2 (April, 1988).
- [32] E. Miescher and K. P. Huber, in *International Review of Science*, Physical Chemistry, Series 2, edited by A. D. Buckingham (Butterworth, London, 1975), Vol. 1, and references therein.
- [33] Calculations on energy levels of  $X^2\Pi^+$ ,  $B^2\Pi^+$ ,  $C^2\Pi^+$ , and  $D^2\Sigma^+$  states are based on constants provided by K. P. Huber and G. Herzberg in *Constants of Diatomic Molecules* (Van Nostrand Reinhold Company, New York, 1979).
- [34] J. A. Guest and L. C. Lee, *J. Phys. B* **14**, 3401 (1981).
- [35] D. J. Hart and O. L. Bourne, *Chem. Phys.* **133**, 103 (1989).
- [36] D. Zakheim and P. Johnson, *J. Chem. Phys.* **68**, 3644 (1978).
- [37] P. Cremaschi, *J. Chem. Phys.* **75**, 3944 (1981).